Design and evaluation of a pulsed-jet chirped-pulse millimeter-wave spectrometer for the 70-102 GHz region

Design and evaluation of a pulsed-jet chirped-pulse millimeter-wave spectrometer for the 70–102 GHz region

G. Barratt Park,[1] Adam H. Steeves,[1,a)] Kirill Kuyanov-Prozument,[1] Justin L. Neill,[2] and Robert W. Field[1,b)]
[1]*Department of Chemistry, Massachusetts Institute of Technology, Cambridge, Massachusetts 02139, USA*
[2]*Department of Chemistry, University of Virginia, Charlottesville, Virginia 22904, USA*

(Received 6 April 2011; accepted 15 May 2011; published online 8 July 2011)

Chirped-pulse millimeter-wave (CPmmW) spectroscopy is the first broadband (multi-GHz in each shot) Fourier-transform technique for high-resolution survey spectroscopy in the millimeter-wave region. The design is based on chirped-pulse Fourier-transform microwave (CP-FTMW) spectroscopy [G. G. Brown, B. C. Dian, K. O. Douglass, S. M. Geyer, S. T. Shipman, and B. H. Pate, Rev. Sci. Instrum. **79**, 053103 (2008)], which is described for frequencies up to 20 GHz. We have built an instrument that covers the 70–102 GHz frequency region and can acquire up to 12 GHz of spectrum in a single shot. Challenges to using chirped-pulse Fourier-transform spectroscopy in the millimeter-wave region include lower achievable sample polarization, shorter Doppler dephasing times, and problems with signal phase stability. However, these challenges have been partially overcome and preliminary tests indicate a significant advantage over existing millimeter-wave spectrometers in the time required to record survey spectra. Further improvement to the sensitivity is expected as more powerful broadband millimeter-wave amplifiers become affordable. The ability to acquire broadband Fourier-transform millimeter-wave spectra enables rapid measurement of survey spectra at sufficiently high resolution to measure diagnostically important electronic properties such as electric and magnetic dipole moments and hyperfine coupling constants. It should also yield accurate relative line strengths across a broadband region. Several example spectra are presented to demonstrate initial applications of the spectrometer. © *2011 American Institute of Physics*. [doi:10.1063/1.3597774]

I. INTRODUCTION

Microwaves and millimeter waves are powerful tools for the spectroscopic study and state-specific detection of gas-phase molecules. The advantage of these spectral regions derives primarily from the extremely high resolution and accompanying high frequency accuracy that they provide. The millimeter-wave region has proven particularly important for measurements on small molecules with large rotational constants,[1–3] studies of pure-electronic Rydberg-Rydberg transitions,[4–9] sensitive detection of molecules at room temperature,[10–12] and detection of astronomical molecules.[13]

Much recent progress has been made in the development of methodology for gas-phase millimeter-wave spectroscopy. Traditional frequency-domain spectrometers must be scanned one frequency element at a time, which makes the acquisition of broadband chemically-relevant spectra expensive and time-consuming, especially when used in conjunction with 10–20 Hz repetition rate supersonic jet molecule sources and Nd:YAG-pumped tunable lasers. A tremendous advantage has been obtained in frequency-domain millimeter and sub-millimeter spectroscopy by using fast sweeps, which can measure up to 5×10^5 resolved spectral features per second (typically 50–500 GHz/s).[14–18] Efforts have also been made to apply fast sweep techniques to pulsed nozzle experiments.[19,20] However, because the pulse durations in those experiments are typically not more than 10–100 times longer than the $\sim$1 μs time constant of the bolometer detectors used, such methods cover no more than approximately 100 resolution elements (typically 10 MHz) per gas pulse. Furthermore, the method is not suited for spectroscopy on laser-excited states with lifetimes that are short relative to the time constant of the detector.

Cavity-enhanced Fourier-transform microwave spectrometers caused a major breakthrough starting in the early 1980s.[21–25] A few cavity-enhanced Fourier transform spectrometers have been reported above 50 GHz.[26–31] However, the high quality factor of the Fabry-Perot cavity used in such spectrometers limits each Fourier-transform acquisition to a few MHz. While these spectrometers can be used to cover wide frequency ranges at high resolution and high sensitivity, they must do so in a sequence of many narrowband acquisitions, and the cavity resonance frequency must be mechanically tuned at each step.

The recent invention by Pate and co-workers of chirped-pulse Fourier-transform microwave (CP-FTMW) spectroscopy has made possible acquisition of truly broadband (>10 GHz per pulse) Fourier-transform spectra in the microwave region ($\sim$8–18 GHz).[32–34] The invention makes use of recent advances in broadband microwave electronics. In the University of Virginia implementation, a 24 GS/s arbitrary waveform generator is used to generate a broadband,

a)Present address: Department of Pharmaceutical Chemistry, University of California, San Francisco, California 94143, USA.
b)Author to whom correspondence should be addressed. Electronic mail: rwfield@mit.edu.

frequency-chirped pulse, which is up-converted and amplified to ~300 W in a traveling wave tube amplifier. The resulting high-power chirped pulse interacts with a molecular sample, polarizing all the transitions that lie within the bandwidth of the chirp. The sample emits a broadband free induction decay (FID) signal, which is detected directly by a fast 20 GHz oscilloscope. Further work at the University of Virginia has been done to implement the technique at frequencies up to 40 GHz.[35]

We have built a chirped-pulse millimeter-wave (CPmmW) spectrometer that operates in the 70–102 GHz region. CPmmW spectroscopy takes advantage of recent advances in broadband millimeter-wave amplifiers and heterodyne receivers. The design is similar to that of Pate and co-workers, but the output of the arbitrary waveform generator is up-converted and multiplied to millimeter-wave frequencies. After the FID is collected, it is down-converted to the broadband DC-12 GHz region so that it can be detected directly and averaged in the time domain by a fast oscilloscope. In spite of the advantages that are offered by CPmmW spectroscopy, there are also several challenges associated with operating at higher frequency, particularly lower available power and faster dephasing. Here, we address some of these challenges and demonstrate the abilities of our current spectrometer.

II. SPECTROMETER DESIGN

The spectrometer is based on the CP-FTMW spectrometer of Pate and co-workers.[32] A schematic of the CPmmW spectrometer design is shown in Fig. 1. A 4.2 GS/s arbitrary waveform generator (AWG) is used to generate chirped pulses at frequencies in the range of 0.2–2 GHz. These pulses are up-converted by mixing with a phase-locked 10.7 GHz oscillator, and one of the sidebands is selected using a bandpass filter. Access to the millimeter-wave region is achieved by active multiplication (×8) of the resulting chirped microwave pulse. Because frequency multipliers multiply both the carrier frequency and the bandwidth of a chirped pulse, it is possible to generate chirped millimeter-wave pulses with ~15 GHz bandwidth starting with a 0.2–2 GHz microwave pulse. As a result, the bandwidth of the AWG used in the experiment may be much narrower than that of the desired millimeter-wave chirped pulse. This was noted by Brown *et al.* in the bandwidth extension scheme designed for the FT-CPMW spectrometer.[32]

Unlike the spectrometer of Pate and co-workers, which uses a traveling wave tube amplifier to achieve peak pulse powers of up to 300 W, the CPmmW spectrometer power is limited by the capabilities of currently available broadband E- and W-band amplifiers, which can attain peak powers of only ~10–100 mW. Our system uses an active frequency doubler with an output power of 30 mW. Because the millimeter-wave power is low, horn antennas can be safely located outside of the molecular beam chamber. Teflon optics are used to focus the millimeter-wave radiation into the chamber through a set of teflon windows.

The molecular FID must be down-converted to microwave frequencies for direct detection on a fast oscilloscope. This is achieved by mixing the collected signal with the output of a W-band Gunn oscillator. The detection bandwidth is limited by the 12 GHz oscilloscope [Tektronix model TDS6124C] used in the experiment. As in the design of Pate and co-workers, all oscillators and clocks used in the experiment are phase locked to the same 10 MHz frequency standard. The experiment is repeated at an exact integer multiple of the period of the 10 MHz reference. This ensures that the phase of the chirped pulse and the resultant FID is constant from pulse to pulse so that the signal can be phase-coherently averaged on an oscilloscope in the time domain.

III. POWER LIMITATION

A. Measurement of effective power

The available power for the CPmmW spectrometer is currently limited to about 30 mW by the capabilities of

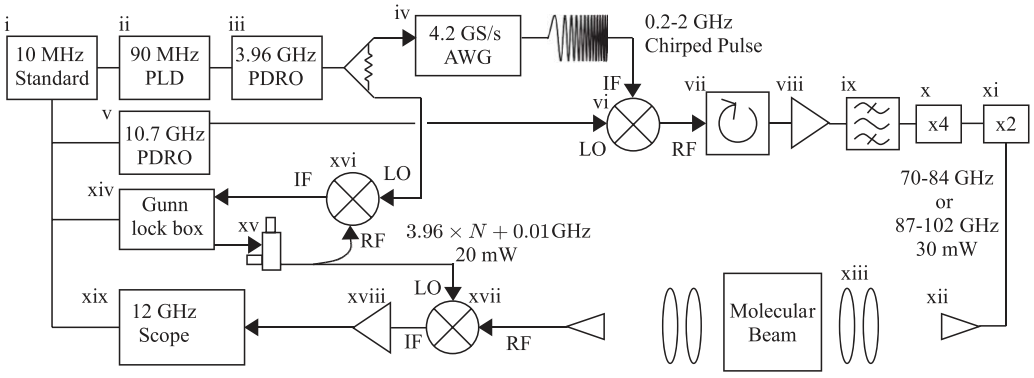

FIG. 1. Schematic diagram of the CPmmW instrument. For a full list of parts, see the Appendix. All components of the experiment are phase locked to the same 10 MHz Rubidium frequency standard (i). A 4.2 GS/s AWG [Tektronix model AWG710B] (iv), operating at the 3.96 GHz rate of an external clock (iii), is used to generate a linearly-chirped pulse, which is up-converted (vi) by mixing with the output of a fixed-frequency 10.7 GHz oscillator (v). The resultant signal is isolated (vii) and amplified (viii). The desired sideband is then selected using a bandpass filter (ix) and actively frequency-multiplied by a factor of 8 (x and xi) to produce a chirped pulse that covers the 70–84 GHz or the 87–102 GHz frequency range with a peak power of 30 mW. The millimeter-wave pulse is coupled into free space using a 24 dBi standard gain horn (xii) and focused into a molecular beam chamber by a pair of teflon lenses (xiii). After the chirped excitation pulse has polarized the molecular sample, the FID is collected and down-converted (xvii) by mixing with the output of a Gunn oscillator (xv). The resultant signal is input to a low-noise amplifier (xviii) and averaged in the time domain on a 12 GHz oscilloscope (xix).

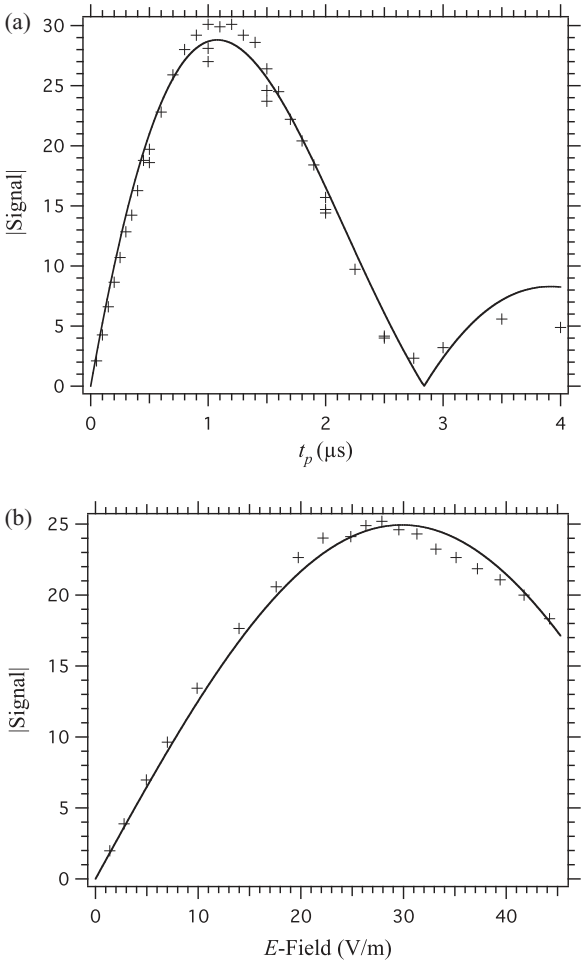

FIG. 2. (a) The amplitude of the FID signal from the SO_2 $6_{06} \leftarrow 5_{15}$ transition is plotted as a function of the duration of the single frequency excitation pulse. The data were fit to Eq. (1) to obtain best-fit parameters $\tau = 2.3 \pm 0.2$ μs and $\omega_R = 1.11 \pm 0.04$ MHz. (b) The signal amplitude from the same transition is plotted as a function of millimeter-wave pulse power attenuation, for a constant pulse duration of $t_p = 2$ μs. The solid curve is the signal amplitude predicted by Eq. (1) with the best-fit parameters from above. The E-field plotted on the x-axis was calculated from the best-fit value of ω_R at zero attenuation and scaled according to the variable attenuation.

commercially-available broadband millimeter-wave amplifiers. As millimeter-wave technology develops, more power is expected to become available in broadband solid-state devices. However, because of power limitations, it is important to achieve efficient coupling of power into the molecular beam chamber so that the E-field of the radiation that interacts with the molecules is as high as possible. In order to evaluate the effective E-field in the interaction region, test measurements were performed on the $6_{06} \leftarrow 5_{15}$ b-type pure rotational transition in SO_2 at 72.758 GHz, for which the transition dipole moment (averaged over M_J components) is 0.83 D. A resonant single-frequency pulse of varying duration was used to excite the transition.

The results, shown in Fig. 2, can be compared to an exponentially-damped Rabi oscillator. The detected signal, S, is the E-field radiated by the molecules, which is proportional to the magnitude of the quantum coherence, $|a_0 a_1|$, evaluated at time t_p, the pulse duration:

$$S \propto |a_0(t_p)a_1(t_p)| = \exp\left(\frac{-t_p}{\tau}\right)|\sin(\omega_R t_p)|. \tag{1}$$

In Eq. (1), $\omega_R = \mu\mathcal{E}/\hbar$ is the on-resonance Rabi frequency and $1/\tau$ is the decay rate of the coherence.

The data shown in Fig. 2 were fit to Eq. (1) to obtain best-fit parameters of 2.3 ± 0.2 μs for τ and 1.11 ± 0.04 MHz for ω_R. The fit parameter for τ agrees with the measured 2.1 μs $1/e$ dephasing time of the transition, which is dominated by the Doppler effect. The measured Rabi frequency corresponds to an effective E-field of 42 V/m. The measured diameter of the millimeter-wave focus (containing 90% of the integrated E-field) from the teflon lenses is ~2.5 cm. If 30 mW of power were ideally focused onto a $(2.5\text{ cm})^2$ area, it would result in a 195 V/m E-field. Part of the loss of effective E-field is due to power loss. There are unavoidable losses due to reflections in the horn antenna and from the surfaces of the lenses and chamber windows. However, horn-to-horn transmission loss is only ~3 dB (corresponding to a loss of 30% in E-field). The remaining loss of effective E-field can be attributed to imperfections in the profile and focussing of the millimeter-wave beam.

B. Power requirements for broadband chirped pulses

To calculate the achievable polarization of a two-level system excited by a broadband chirped millimeter-wave pulse, we integrate the optical Bloch equations for the case of a linearly-chirped pulse, as given by McGurk *et al.*[36] We define the polarization in the form

$$P = (P_r + iP_i)e^{i(\omega t - kz)} + \text{c.c.} \tag{2}$$

The time-dependent E-field of the excitation pulse is

$$\begin{aligned} E &= 2\mathcal{E}\cos\left(\omega_i t + \frac{1}{2}\alpha t^2\right) \\ &= 2\mathcal{E}\cos\{[\omega_0 - \Delta\omega(t)]\,t\}, \end{aligned} \tag{3}$$

where we define α as the linear frequency sweep rate and $\Delta\omega$ as the detuning of the excitation pulse from the two-level system resonance, ω_0. The Bloch equations can be written for the polarization in terms of $\Delta\omega$ (Ref. 36):

$$\begin{aligned} \alpha\frac{dP_r}{d(\Delta\omega)} + \Delta\omega P_i + \frac{P_r}{T_2} &= 0 \\ \alpha\frac{dP_i}{d(\Delta\omega)} - \Delta\omega P_r + \frac{\mu^2\mathcal{E}}{2\hbar}\Delta N + \frac{P_i}{T_2} &= 0 \\ \frac{\alpha\hbar}{4}\frac{d(\Delta N)}{d(\Delta\omega)} - \frac{\mathcal{E}}{2}P_i + \frac{\hbar}{4}\frac{(\Delta N - \Delta N_0)}{T_1} &= 0. \end{aligned} \tag{4}$$

In Eq. (4), T_1 and T_2 are the familiar decay lifetimes of the population and coherence, respectively, and ΔN is the population difference. Equation (4) was numerically integrated and the results are shown in Fig. 3.

Figure 3 demonstrates that the polarization achievable in a typical small molecule across a bandwidth of 10 GHz

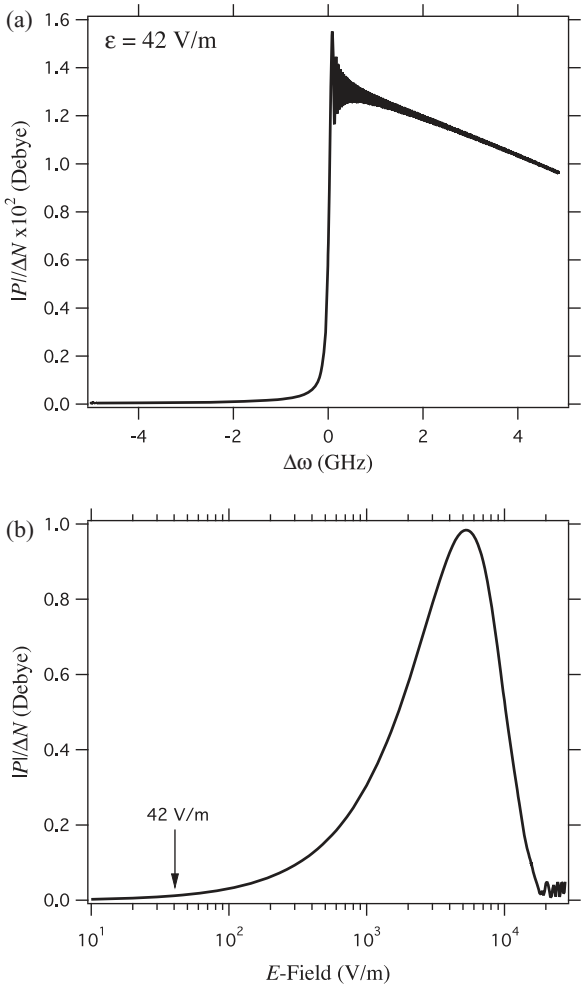

FIG. 3. Equation (4) was numerically integrated for the case of a 10 GHz bandwidth chirped pulse of 1 μs duration exciting a 1 D dipole moment with T_1 and T_2 of 10 μs and 2 μs, respectively. The two level system resonance is assumed to occur at the center of the excitation pulse bandwidth. (a) The integration of Eq. (4) is shown for the above parameters with an E-field of 42 V/m, which is the available E-field in the current spectrometer. The magnitude of the polarization is plotted. (b) The E-field ($\mathcal{E}$) was varied and the resultant polarization after the excitation pulse is plotted. Optimal polarization occurs at an E-field of ~4000 V/m. The polarization never quite reaches its maximum value of 1 D because a small amount of dephasing occurs during the excitation pulse. Note that the polarization achieved at 42 V/m corresponds to only ~1.5% of the maximum achievable polarization.

with a 42 V/m electric field is only 1% of the maximum polarization that would be achievable if higher chirped-pulse power were available. A qualitative difference between the polarization achieved with a broadband chirped pulse and that achieved with a single-frequency excitation pulse (Figure 2) is that even in the absence of relaxation effects, recurrence of the polarization does not take place at high E-field in the chirped-pulse case. This is a well known phenomenon in the adiabatic fast passage regime. When $\mu\mathcal{E}/\hbar\sqrt{\alpha} \gg 1$, the effective E-field vector in the Bloch polarization picture is very strong and moves slowly relative to the Rabi precession. The polarization vector precesses tightly around the E-field vector as it is swept through 180°, and the system is swept slowly through resonance until population inversion is achieved.[37]

In the weak field case ($\mu\mathcal{E}/\hbar\sqrt{\alpha} \ll 1$), the signal scaling has been solved by McGurk *et al.*[36] They found that

$$P \propto \frac{\mu^2 \mathcal{E} \Delta N}{\sqrt{\alpha}}. \tag{5}$$

The polarization will also decay at a rate proportional to $T_1^{-1} + T_2^{-1}$. Therefore, the excitation must occur on a timescale short compared to these time constants. Given that the excitation pulse duration is constrained, the obtainable signal is proportional to the reciprocal square root of the bandwidth. As pointed out by Brown *et al.*,[32] this means that the chirped-pulse signal scales favorably as bandwidth is increased. In contrast, the signal obtained from a Fourier-transform limited pulse scales as the reciprocal of the bandwidth to the first power. It is possible to achieve more polarization from a given transition by decreasing the bandwidth of the chirped pulse. However, this is rarely an advantageous strategy for increasing the efficiency of spectral acquisition, because the increase in signal is only proportional to $\Delta\omega^{(1/2)}$. Breaking up a spectrum into more than one frequency region therefore does not decrease the averaging time needed to obtain a specified signal-to-noise level over a given frequency region, since the noise reduction also scales as the square root of the number of averages, and there is a cancelation between the signal increase and the required number of averages.

In the strong power regime (where $\mu\mathcal{E}/\hbar\sqrt{\alpha}$ is no longer $\ll 1$), the maximum achievable polarization is limited by $P_{max} = \mu\Delta N$. The maximum obtainable polarization from a given sample does not scale with the chirp bandwidth or the E-field, and only scales as μ to the first power.

IV. SHORTER DEPHASING TIMES

In addition to low power availability, another challenge that faces chirped-pulse spectroscopy in the millimeter-wave region is that the dephasing time of the molecular transitions tends to be much shorter than in the centimeter-wave region. In a supersonic expansion, the most significant contributor to the lifetime of the FID is usually the Doppler-limited T_2 broadening. Since the Doppler effect is proportional to the emitted frequency, the dephasing times for the millimeter-wave FIDs are an order of magnitude shorter than those measured with centimeter waves. Pate and co-workers report FID lifetimes of ~10 μs below 20 GHz,[32,33] while we encounter lifetimes of ~2 μs. As a result of the shorter dephasing time, the millimeter-wave chirped pulse must have a shorter duration in order to minimize the dephasing that occurs during the polarizing pulse. This faster dephasing is combined with the additional problem of low available millimeter-wave power, and as a result the CPmmW spectrometer must operate in the low power limit when used to study rotational spectra of molecules with ~1 D dipole moments.

One way to overcome Doppler dephasing in millimeter-wave molecular beam experiments is to change the experimental geometry to reduce the Doppler profile. This has been employed with our CPmmW spectrometer by using a rooftop reflector and a wire-grid polarizer to propagate the millimeter-wave radiation parallel and antiparallel with the molecular beam in a manner similar to that used

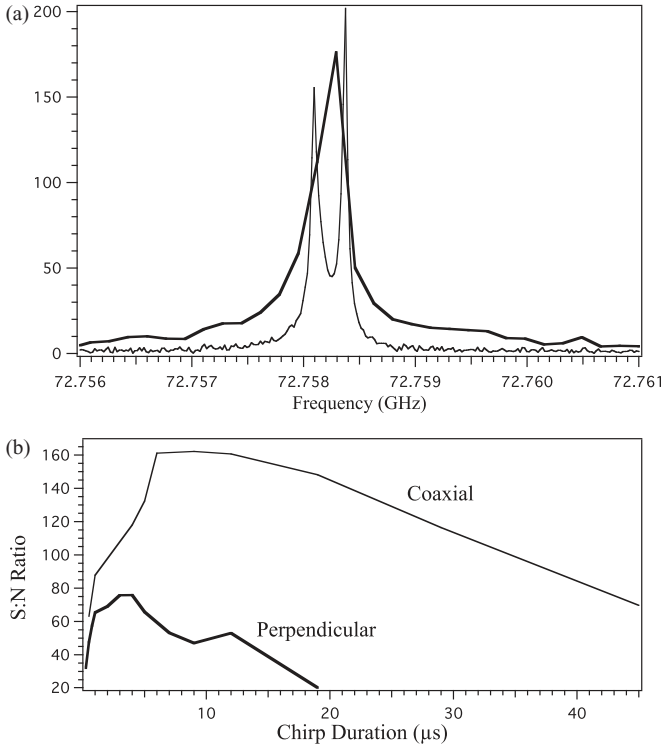

FIG. 4. A comparison is made between the signal obtained from the $6_{06} \leftarrow 5_{15}$ transition of SO_2 in the perpendicular millimeter wave/molecular beam geometry (thick curve) and coaxial geometry obtained using a rooftop reflector (thin curve). The Doppler-limited linewidth is narrower in the coaxial geometry. The line is split into its two Doppler components when this double-pass configuration is used (a). Because the FID lifetime is longer when the Doppler dephasing is minimized, the duration of the excitation chirp can be extended to achieve further improvement in signal strength. In panel (b), the signal-to-background-noise ratio is plotted as a function of the chirp duration for both geometries. The millimeter-wave power, gas expansion characteristics, and other parameters were held constant.

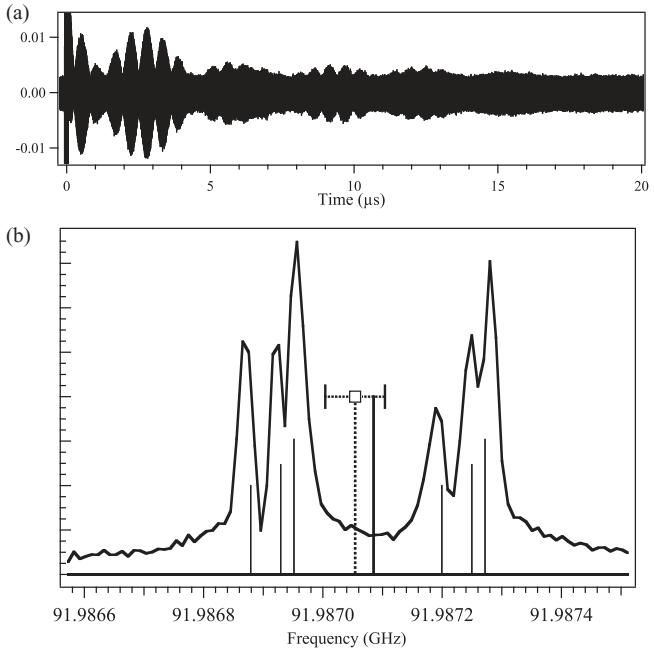

FIG. 5. High-resolution CPmmW spectrum of the acetonitrile $J = 5 \leftarrow 4$, $K = 0$ transition with resolved ^{14}N quadrupole moment hyperfine structure. The FID (a) has a decay constant of ~17 μs. The Hamming window function was used in the Fourier transform. The spectrum (b) is Doppler-doubled as a result of the rooftop reflector geometry. The line spectrum represents the calculated spectrum obtained using the accepted nuclear quadrupole coupling constant, −4.2244 MHz,[39] and a best-fit molecular beam velocity of 508 m/s. The thick central line is the measured central line frequency and the dotted line is the unresolved line position reported by Boucher *et al*. in Ref. 40. The measured line frequency agrees to within the 60 kHz reported uncertainty.

previously to obtain high-resolution spectra with our sequential scanning millimeter-wave absorption spectrometer.[38] The co-propagating geometry removes most of the Doppler effect caused by the component of the molecular velocity perpendicular to the molecular beam direction. In Fig. 4, a comparison is made between the signal obtainable with and without the rooftop reflector geometry. The linewidth was reduced from 350 kHz to 66 kHz. Because the FID lifetime is lengthened by a factor of 5, it is possible to extend the chirp duration without loss due to dephasing. This leads to stronger polarization of the sample and more signal. Additional advantage in the signal-to-background-noise ratio arises from the fact that the line is narrower.

The coaxial geometry can also be used to improve the resolution, as demonstrated in the case of the $J = 5 \leftarrow 4$, $K = 0$ transition of acetonitrile with resolved hyperfine structure due to the ^{14}N quadrupole moment (Fig. 5).

V. PHASE STABILITY

Another difficulty with up-converting the chirped-pulse technique into the millimeter-wave region is that the experiment becomes more sensitive to phase instabilities. When the signal is frequency-multiplied by 8, any phase jitter is also multiplied by 8. Phase jitter might be attributed to temperature fluctuations and mechanical vibrations in the laboratory, or to phase jitter characteristics of electrical components.

When using chirped-pulse techniques, two types of phase jitter are possible: t-jitter as illustrated in Eq. (6a) or ϕ-jitter, as illustrated in Eq. (6b):

$$I \propto \sin\left[\omega_0(t + \Delta t) + \frac{1}{2}\alpha(t + \Delta t)^2 + \phi\right], \tag{6a}$$

$$I \propto \sin\left[\omega_0 t + \frac{1}{2}\alpha t^2 + (\phi + \Delta\phi(\omega))\right]. \tag{6b}$$

We find that when the phase of the FID is unstable from one acquisition to the next, the instability can be corrected by rotating the phases of the Fourier transforms relative to one another (and not by shifting the FIDs in time). Furthermore, we find that the rotation angle that maximizes the overlap between the two Fourier transforms is independent of the frequency. That is, in Eq. (6b), $\Delta\phi(\omega) = \Delta\phi$. Thus, Eq. (7) can be used to rotate the phase of the Fourier transform to correct for phase instabilities:

$$\begin{pmatrix} \Re\{F'(\omega)\} \\ \Im\{F'(\omega)\} \end{pmatrix} = \begin{pmatrix} \cos\Delta\phi & \sin\Delta\phi \\ -\sin\Delta\phi & \cos\Delta\phi \end{pmatrix} \begin{pmatrix} \Re\{F(\omega)\} \\ \Im\{F(\omega)\} \end{pmatrix}, \tag{7}$$

where $\Re\{F(\omega)\}$ and $\Im\{F(\omega)\}$ refer to the real and imaginary parts of the Fourier transform, respectively.

The frequency-independence of the correction indicates that the source of the phase instability is likely to be in one of the single-frequency local oscillators. If the phase jitter were generated in a component that passes a chirped pulse, there would likely be frequency dependence to the phase jitter, since different frequencies accumulate phase at different rates. In future generations of our spectrometer, we plan to replace the Gunn oscillator with a multiplied phase-locked microwave oscillator as the local oscillator for the down-conversion. This will allow us to determine whether the Gunn oscillator is the source of phase instability.

Long-term drifts in phase of the type discussed above have been efficiently corrected in signal processing. This type of instability can be corrected by rotating the phase of the Fourier transform of each acquisition (Eq. (7)) by the angle $\Delta\phi$ that maximizes the overlap of the strongest line in the spectrum. Because of the frequency independence of $\Delta\phi$, this rotation maximizes the phase overlap of all molecular lines, regardless of how far apart they are in frequency. When it is necessary to perform a long average over the course of an hour or more, the averaging can be performed in shorter 5–10 min acquisitions over which time the phase of the FID is stable. These shorter acquisitions can then be phase corrected with signal processing tools before being averaged together. The overall time required for the acquisition of the long average is affected negligibly because the data must be Fourier-transformed and stored only once every 5–10 min when this scheme is implemented.

A disadvantage of this method is that it is only efficient when there is a strong line that is visible above the baseline noise after a 5–10 min acquisition. If necessary, the phase correction can be achieved by introducing into the sample mixture a standard that has a strong transition. The phase-correction algorithm can be applied automatically in the LABVIEW program that is used to collect and average the data.

As an example, we have acquired 87–92 GHz spectra of the 193 nm photolysis products of acrylonitrile. We collected 28 000 averages in acquisitions of 500–2000 averages each. In Fig. 6, we present a comparison between the spectra obtained when each acquisition is phase corrected and when each acquisition is not phase corrected. Note that the levels of background noise in the two spectra are similar, but the signal in the phase-corrected spectrum is several times stronger, because signal is destroyed when individual FIDs are averaged out of phase. In the phase-corrected spectrum, the signal-to-background-noise ratio increases as the square root of the number of acquisitions out to the longest measurement of 28 000 acquisitions.

VI. EVALUATION

A. Spectroscopy of ground states

We used the frequency region surrounding the 72 976.7794 MHz OCS $J = 6 \leftarrow 5$ transition to compare the CPmmW spectrometer to the supersonic jet W-band bolometer-detected absorption spectrometer used previously in the Field laboratory (Fig. 7).[38,41] The older absorption

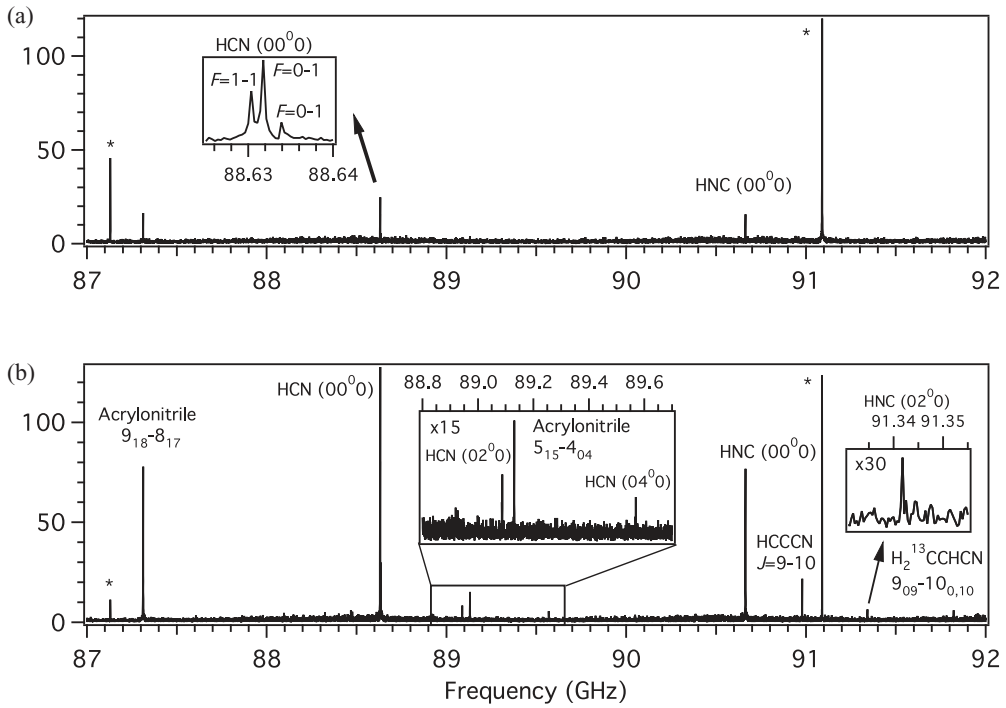

FIG. 6. A 5-GHz bandwidth spectrum of the 193 nm photolysis products of acrylonitrile was acquired in a supersonic jet expansion. A total of 28 000 averages were recorded in short acquisitions of 500–2000 averages each. Without phase correction (a), only the acrylonitrile $J_{K_aK_c} = 9_{18} \leftarrow 9_{17}$, the HCN $(v_1\, v_2^{\ell}\, v_3) = (0\,0^0\,0)$, $J = 1 \leftarrow 0$ line, and the HNC $(0\,0^0\,0)$, $J = 1 \leftarrow 0$ lines are detected above the noise. When the phase of each spectrum is shifted to maximize the overlap of the HCN $(0\,0^0\,0)$ line (b), the signal-to-background-noise ratio increases dramatically and more lines become visible: HCN $(0\,2^0\,0)$, $J = 1 \leftarrow 0$; HCN $(0\,4^0\,0)$, $J = 1 \leftarrow 0$; HNC $(0\,2^0\,0)$, $J = 1 \leftarrow 0$; acrylonitrile $5_{15} \leftarrow 4_{04}$; HCCCN, $J = 10 \leftarrow 9$ and a ^{13}C-substituted acrylonitrile line at 91 821.43 MHz. Artifact lines corresponding to local oscillator frequencies are labeled with asterisks.

spectrometer was used primarily for measuring hyperfine structure surrounding lines with known positions and was not designed for broadband spectral acquisition. With the absorption spectrometer, only a narrow 100 MHz region containing the main OCS $J = 6 \leftarrow 5$ transition could be scanned during the 100 min experiment (Fig. 7(a)). However, with the CPmmW spectrometer, a 4 GHz spectral region could be surveyed at improved signal-to-background-noise ratio in approximately half the time. The strong OCS $J = 6 \leftarrow 5$ transition is visible above the background noise after only seconds of averaging. After 5 min of averaging, the spectrum reaches a signal-to-background-noise ratio comparable to that obtained with the absorption spectrometer. The spectrum shown in Fig. 7(b) was obtained in 50 min and exhibits greater than two-fold improvement in signal-to-background-noise ratio over the spectrum shown in Fig. 7(a). Because the broadband Fourier-transform capabilities of the CPmmW spectrometer can be used to survey a broad spectral region, it is possible not only to find the strong OCS $J = 6 \leftarrow 5$ transition after mere seconds of averaging, but also to observe simultaneously the weaker satellite transitions, which are assigned to isotopes and vibrationally excited states of OCS. From the signal-to-background-noise ratio of the $O^{13}CS$ peak, we estimate that for the bandwidth and acquisition time used in this experiment, the limit of detection for OCS $J = 6 \leftarrow 5$ transition is $\sim 10^{11}$ molecules/cm^3.

The CPmmW spectrometer has also been used in millimeter wave-optical double resonance (mmODR) experiments. In the first such implementation, the millimeter-wave beam was crossed with the frequency-doubled output of a pulsed dye laser. The supersonic jet expansion was directed at a right angle to the millimeter-wave and laser beams. The $6_{06} \leftarrow 5_{15}$ transition in ground-state SO_2 was excited by the millimeter waves and the laser frequency was scanned across the $\tilde{C}\ ^1B_2(1, 3, 2) \leftarrow \tilde{X}\ ^1A_1(0, 0, 0)$ band centered at 45 336 cm^{-1}. The ~10 ns laser pulse arrived 500 ns after the start of the millimeter-wave FID, so that it causes a decrease in the magnitude of the millimeter-wave coherence if it is resonant with one of the two states involved. The method is similar to the cavity Fourier-transform microwave-optical double resonance technique of Nakajima *et al.*[42] The double resonance spectrum was obtained by recording the normalized ratio of the FID intensity before and after the laser pulse. The double resonance spectrum is plotted along with the laser induced fluorescence (LIF) spectrum in Fig 8. Rotational assignments for this band have been made previously by Yamanouchi *et al.*[43] The double resonance peak at 45 332.65(2) cm^{-1} agrees to within experimental uncer-

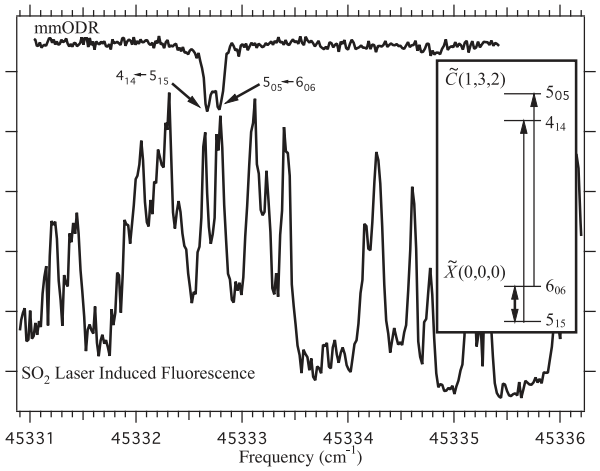

FIG. 8. The LIF spectrum of SO_2 (lower trace) to the (1, 3, 2) level of the $\tilde{C}$ state is shown along with a millimeter wave-optical double resonance spectrum to the same band (upper trace). The scheme for the double resonance experiment is shown in the inset. The thick double arrow represents the millimeter-wave coherence that was generated between the 6_{06} and 5_{15} rotational levels of the $\tilde{X}(0, 0, 0)$ state. The double resonance signal was obtained by measuring the dip in the millimeter-wave FID intensity as the laser was scanned.

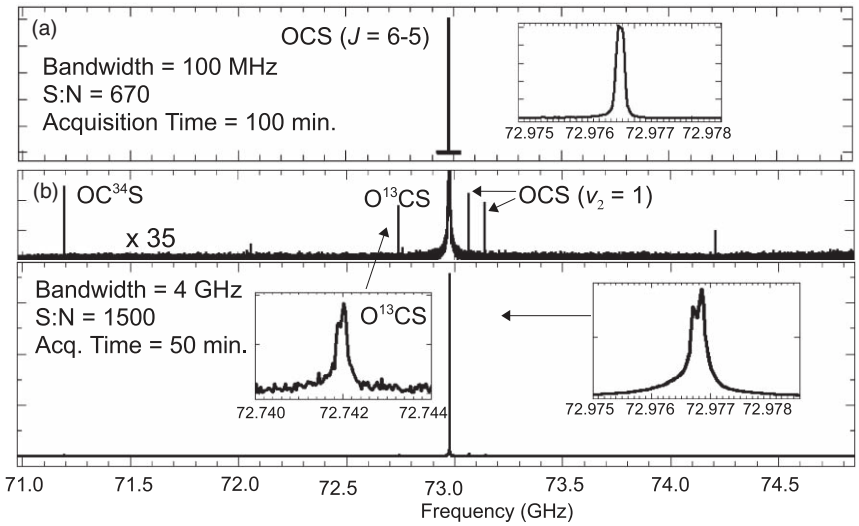

FIG. 7. For comparison, the spectrum of OCS in the region surrounding the $J = 6 \leftarrow 5$ region was measured with (a) the scanned absorption spectrometer previously used in the Field group and (b) the CPmmW spectrometer. The CPmmW spectrometer was able to cover 40 times the bandwidth in half the time with better signal-to-background-noise ratio. Differences in line profile are due primarily to the fact that the CPmmW spectrometer detects electric field, which is proportional to the square root of power.

tainty with the peak assigned to the $4_{14} \leftarrow 5_{15}$ transition. We have assigned the other peak at 45 332.79(2) cm^{-1} to the $5_{05} \leftarrow 6_{06}$ transition, which was not assigned by Yamanouchi *et al*. due to the spectral congestion and complications caused by Coriolis effects. Both of our assignments are confirmed by the existence of combination difference peaks in the LIF spectrum.

The successful implementation of mmODR with our spectrometer suggests that the technique could be used to generate two dimensional chirped-pulse mmODR spectra in order to decongest LIF spectra and provide rotational assignments. The technique will provide the most information for molecules with sufficiently small rotational constants such that the chirped pulse will cover several rotational transitions. The laser spectrum can be scanned while many ground-state rotational transitions are probed, and the Fourier transform of the FID dip will provide information about which ground-state rotational level is involved in each LIF transition.

B. Spectroscopy of laser-excited states

CPmmW spectroscopy is particularly advantageous as a tool for probing laser-excited states since it is designed for pulsed operation and can be easily coupled to pulsed supersonic jets and tunable pulsed laser systems. The duty cycle of such experiments is necessarily low. In our laboratory, the pulsed dye lasers operate at 10 Hz and the chirped-pulse experiment lasts ~5 μs or less. Thus the fraction of time when microwave observations can be made is less than 10^{-4}, when compared with traditional non-pulsed absorption measurements. CPmmW spectroscopy is well suited to this case since it can record a broad spectral region during the short radiative lifetime and the time between gas pulses can be used for digital averaging of the FID.

As a demonstration that CPmmW spectroscopy can be used to probe laser-excited states, we measured the $(J' = 2, N' = 2) \leftarrow (J' = 1, N' = 1)$ transition in the excited triplet electronic state $e\ ^3\Sigma^-$ $(v = 2)$ of CS using a 1 GHz bandwidth chirped pulse (Fig. 9). Because the uncertainty in laser transitions is typically ~1 GHz, it may be necessary to cover a broad spectral range when probing for rotational transitions of laser-excited states. The CS line could be seen above the noise after about 100 averages (10 s). We estimate that this signal came from a total of $\sim 4.8 \times 10^{10}$ excited CS molecules in a single quantum state.

The transition frequency was previously reported as 76 229.027(20) MHz.[44] In the current work, we correct this frequency to 76 263.89(10). The FWHM is 1.1 MHz and is attributable to the radiative lifetime of the $e\ ^3\Sigma^-$ state. The difference between the previously reported frequency and the current value is almost exactly 35 MHz, which was the reference frequency used in the original measurement to stabilize the Gunn oscillator. This suggests that the oscillator may have been erroneously locked to the second harmonic of the reference.

The CPmmW technique has also been recently applied to pure electronic Rydberg-Rydberg transitions in calcium atoms.[9]

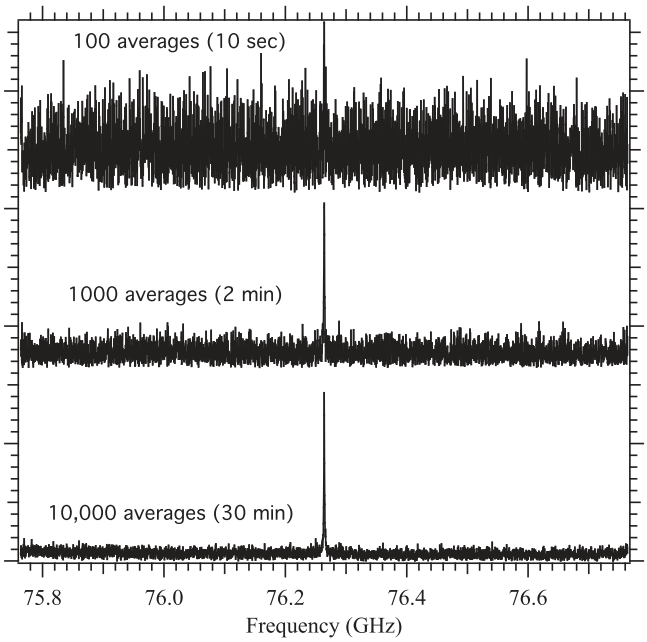

FIG. 9. The $e\ ^3\Sigma^-$ $(v = 2)$ state of CS was populated using the frequency-doubled output of a tunable Nd:YAG-pumped dye laser at ~39 910 cm^{-1}. The $(J' = 2, N' = 2) \leftarrow (J' = 1, N' = 1)$ transition in the excited state was then probed using a 1 GHz bandwidth chirped pulse centered on the transition.

VII. INSTRUMENT NOISE FLOOR

In our current spectrometer, the noise level is set by the noise output of the source amplifier. We experimentally measure the noise level at the receiver to be a factor of 9 in power above the thermal noise at the receiver. Fast, broadband PIN switches with insertion losses of ~2 dB have recently become available for the W-band. We plan to place a switch after the source amplifier to eliminate source amplifier noise during detection of the FID. The noise encountered in the experiment will then be set by the noise figure of the detection arm. In the current spectrometer, the noise figure of the detection arm is set by a combination of a rather lossy downconverter (9 dB conversion loss) and the 2.3 dB noise figure of the low noise amplifier for the RF. The combined noise figure after the collection horn is, therefore, ~11.3 dB (or a factor of 13.5). Recently, low-noise amplifiers (LNAs) covering the full W-band with a noise figure of ~5 dB have become available. Such an amplifier would need to be protected from the powerful excitation pulse by a switch (~2 dB insertion loss). The combined noise figure of the detection arm would then be set by these two components to 7 dB (or a factor of 5.0). We therefore expect to be able to achieve an overall reduction in noise floor by a factor of $13.5 \times 9/5.0 = 24$ in power or 4.9 in electric field. The 2 dB insertion loss of the switch on the source will cause a 25% loss in signal, but this will be more than compensated by the reduction in noise floor.

VIII. FUTURE WORK

CPmmW spectroscopy is shown to be an advantageous method for spectroscopy in the 70–100 GHz region. However, future work is planned to improve the sensitivity of

the method by taking full advantage of recent advances in millimeter-wave technology. Most importantly, we plan to obtain W-band low-noise amplifiers and switches to improve the noise floor of the detection arm, as discussed in Sec. VII. We also hope to obtain new power amplifiers to increase the strength of our excitation pulse.

Technology is rapidly progressing for broadband millimeter-wave power amplifiers. Powers up to 400 mW have been reported across the W-band.[45,46] Because signal scales with the square root of pulse power, such an amplifier (used in conjunction with a 2 dB insertion loss switch) would improve the signal strength in the CPmmW spectrometer by a factor of 3.

ACKNOWLEDGMENTS

The authors are grateful for advice and support from Brooks Pate and his lab. This work was supported at MIT by DOE Grant No. DEFG0287ER13671 and by an NSF Graduate Research Fellowship.

APPENDIX: PART LIST

The following part list is labeled with Roman numerals corresponding to the labeling in Fig. 1. In cases where parts are swapped out depending on which sideband is being used, the parts are labeled "a" for the lower (70–85 GHz) sideband and "b" for the upper (87–102 GHz) sideband.

i. 10 MHz Rubidium frequency standard (Stanford Research Systems FS725)
ii. 90 MHz phase-locked crystal oscillator (Miteq PLD-10-90-15P)
iii. 3.96 GHz phase-locked dielectic resonator oscillator (Microwave Dynamics PLO-2000-03.96)
iv. 4.2 GS/s arbitrary waveform generator (Tektronix AWG710B)
v. 10.7 GHz phase-locked dielectric resonator oscillator (Miteq PLDRO-10-10700-3-8P)
vi. Double-balanced mixer (Macom M79)
vii. 8-16 GHz circulator (Hitachi R3113110)
viii. 1.5-18 GHz amplifier (Armatek MH978141)
ix.a. 8.7-10.5 GHz bandpass filter (Spectrum Microwave C9680-1951-1355)
ix.b. 10.9-12.7 GHz bandpass filter (Spectrum Microwave C11800-1951-1355)
x. Q-Band active frequency quadrupler (Phase One Microwave PS07-0153A R2)
xi.a. E-Band active frequency doubler (Quinstar QMM-77151520)
xi.b. W-Band active frequency doubler (Quinstar QMM-9314152ZI1)
xii. WR10 gain horn, 24 dBi gain mid-band (TRG 861W/387)
xiii. Teflon circular lenses, 30 cm and 40 cm focal length at 80 GHz (custom)
xiv. Gunn phase lock module (XL Microwave model 800A)
xv. W-Band Gunn oscillator (J. E. Carlstrom Co.)
xvi. W-Band subharmonic downconverter (Pacific Millimeter Products)
xvii.a. E-Band downconverter (Ducommun Technologies FDB-12-01)
xvii.b. W-Band downconverter (Ducommun Technologies FDB-10-01)
xviii. Low-noise amplifier (Miteq AMF-5D-00101200-23-10P)
xix. 12 GHz Digital storage oscilloscope (Tektronix TDS6124C)

[1] F. C. De Lucia, J. Mol. Spectrosc. **261**, 1 (2010).
[2] J. M. Brown and A. Carrington, *Rotational Spectroscopy of Diatomic Molecules*, Cambridge Molecular Science Series (Cambridge University Press, Cambridge, England, 2003).
[3] W. Gordy and R. L. Cook, *Microwave Molecular Spectra* (Wiley, New York, 1984).
[4] T. R. Gentile, B. J. Hughey, D. Kleppner, and T. W. Ducas, Phys. Rev. A **42**, 440 (1990).
[5] A. G. Vaidyanathan, W. P. Spencer, J. R. Rubbmark, H. Kuiper, C. Fabre, and D. Kleppner, Phys. Rev. A **26**, 3346 (1982).
[6] F. Merkt and A. Osterwalder, Int. Rev. Phys. Chem. **21**, 385 (2002).
[7] A. Osterwalder, A. Wüest, and F. Merkt, J. Chem. Phys. **121**, 11810 (2004).
[8] J. Han, Y. Jamil, D. V. L. Norum, P. J. Tanner, and T. F. Gallagher, Phys. Rev. A **74**, 054502 (2006).
[9] K. Prozument, A. P. Colombo, Y. Zhou, G. B. Park, V. S. Petrović, S. L. Coy, and R. W. Field "Chirped-Pulse Millimeter-Wave Spectroscopy of Rydberg-Rydberg Transitions" (submitted).
[10] B. Leskovar and W. F. Kolbe, IEEE Trans. Nucl. Sci. **26**, 780 (1979).
[11] W. F. Kolbe, W. D. Zollner, and B. Lescovar, Int. J. Infrared Millim. Waves **4**, 733 (1983).
[12] B. S. Dumesh, V. D. Gorbatenkov, V. G. Koloshnikov, V. A. Panfilov, and L. A. Surin, Spectrochim. Acta, Part A **53**, 835 (1997).
[13] *Spectroscopy From Space*, NATO Science Series: II. Mathematics, Physics and Chemistry, Vol. 20, edited by J. Demaisen, K. Sarka, E. A. Cohen (Kluwer Academic, Dordrecht, The Netherlands, 2000).
[14] F. Wolf, J. Phys. D **27**, 1774 (1994).
[15] D. T. Petkie, T. M. Goyette, R. P. A. Bettens, S. P. Belov, S. Albert, P. Helminger, and F. C. De Lucia, Rev. Sci. Instrum. **68**, 1675 (1997).
[16] S. Albert, D. T. Petkie, R. P. A. Bettens, S. P. Belov, and F. C. De Lucia, Anal. Chem. News Features **70**, 719A (1998).
[17] I. Medvedev, M. Winnewisser, F. C. De Lucia, E. Herbst, E. Bialkowska-Jaworska, L. Pszczólkowski, and Z. Kisiel, J. Mol. Spectrosc. **228**, 314 (2004).
[18] I. R. Medvedev, M. Behnke, and F. C. De Lucia, Appl. Phys. Lett. **86**, 154105 (2005).
[19] B. A. McElmurry, R. R. Lucchese, J. W. Bevan, I. I. Leonov, S. P. Belov, and A. C. Legon, J. Chem. Phys. **119**, 10687 (2003).
[20] S. P. Belov, B. A. McElmurry, R. R. Lucchese, J. W. Bevan, and I. Leonov, Chem. Phys. Lett. **370**, 528 (2003).
[21] R. M. Somers, T. O. Poehler, and P. E. Wagner, Rev. Sci. Instrum. **46**, 719 (1975).
[22] T. J. Balle, E. J. Campbell, M. R. Keenan, and W. H. Flygare, J. Chem. Phys. **71**, 2723 (1979).
[23] T. J. Balle and W. H. Flygare, Rev. Sci. Instrum. **52**, 33 (1981).
[24] E. J. Campbell, L. W. Buxton, T. J. Balle, and W. H. Flygare, J. Chem. Phys. **74**, 813 (1981).
[25] J.-U. Grabow, E. S. Palmer, M. C. McCarthy, and P. Thaddeus, Rev. Sci. Instrum. **76**, 093106 (2005).
[26] W. F. Kolbe and B. Leskovar, Rev. Sci. Instrum. **56**, 97 (1985).
[27] W. F. Kolbe and B. Leskovar, Int. J. Infrared Millim. Waves **7**, 1329 (1986).
[28] D. Boucher, R. Bocquet, D. Petitprez, and L. Aime, Int. J. Infrared Millim. Waves **15**, 1481 (1994).
[29] H. Habara, S. Yamamoto, C. Ochsenfeld, M. Head-Gordon, R. I. Kaiser, and Y. T. Lee, J. Chem. Phys. **108**, 8859 (1998).
[30] S. Yamamoto, H. Habara, E. Kim, and H. Nagasaka, J. Chem. Phys. **115**, 6007 (2001).
[31] G. S. Grubbs II, C. T. Dewberry, and S. A. Cooke, "A Fabry-Perot cavity pulsed Fourier transform W-band spectrometer with a pulsed nozzle

source" (62nd Ohio State University International Symposium on Molecular Spectroscopy, 2008).
[32]G. G. Brown, B. C. Dian, K. O. Douglass, S. M. Geyer, S. T. Shipman, and B. H. Pate, Rev. Sci. Instrum. **79**, 053103 (2008).
[33]G. G. Brown, B. C. Dian, K. O. Douglass, S. M. Geyer, and B. H. Pate, J. Mol. Spectrosc. **238**, 200 (2006).
[34]B. C. Dian, G. G. Brown, K. O. Douglass, and B. H. Pate, Science **320**, 924 (2008).
[35]B. H. Pate, personal communication (2011).
[36]J. C. McGurk, T. G. Schmalz, and W. H. Flygare, J. Chem. Phys. **60**, 4181 (1974).
[37]L. Allen and J. H. Eberly, *Optical Resonance and Two-Level Atoms* (Wileys, New York, 1975) Chap. 3.8.
[38]H. A. Bechtel, A. H. Steeves, and R. W. Field, Astrophys. J. Lett. **649**, L53 (2006).
[39]S. G. Kukolich, D. J. Ruben, J. H. S. Wang, and J. R. Williams, J. Chem. Phys. **58**, 3155 (1973).
[40]D. Boucher, J. Burie, A. Bauer, A. Dubrulle, and J. Demaison, J. Phys. Chem. Ref. Data **9**, 659 (1980).
[41]H. A. Bechtel, A. H. Steeves, B. M. Wong, and R. W. Field, Angew. Chem., Int. Ed. **47**, 2969 (2008).
[42]M. Nakajima, Y. Sumiyoshi, and Y. Endo, Rev. Sci. Instrum. **73**, 165 (2002).
[43]K. Yamanouchi, M. Okunishi, Y. Endo, and S. Tsuchiya, J. Mol. Struct. **352/353**, 541 (1995).
[44]A. H. Steeves, H. A. Bechtel, S. L. Coy, and R. W. Field, J. Chem. Phys. **123**, 141102 (2005).
[45]L. A. Samoska, T. C. Gaier, A. Peralta, S. Weinreb, J. Bruston, I. Mehdi, Y. Chen, H. H. Liao, M. Nishimoto, R. Lai, H. Wang, and Y. C. Leong, Proc. SPIE-Int. Soc. Opt. Eng. **4013**, 275 (2000).
[46]T. de Graauw, N. Whyborn, E. Caux, T. Phillips, J. Stutzki, A. Tielens, T. Güsten, F. Helmich, W. Luinge, J. Martin-Pintado, J. Pearson, P. Planesas, P. Roelfsema, P. Saraceno, R. Schieder, K. Wildeman, and K. Wafelbakker, "The Herschel-Heterodyne Instrument for the Far-Infrared (HIFI)," in *Astronomy in the Submillimeter and Far Infrared Domains With the Herschel Space Observatory*, EAS Publication Series, Vol. 34, edited by L. Pagani and M. Gerin, European Astronomical Society (EDP Sciences, Les Ulis, France, 2009) pp. 3–20.